Nickel-Catalyzed Fabrication of SiO_2, TiO_2/Graphitized Carbon, and the Resultant Graphitized Carbon with Periodically Macroporous Structure

Zhibin Lei,*,† Yi Xiao,† Liqin Dang,† Wansheng You,† Gengshen Hu,‡ and Jing Zhang‡

Institute of Chemistry for Functionalized Materials, Faculty of Chemistry and Chemical Engineering, Liaoning Normal University, Dalian, Liaoning 116029, China, and State Key Laboratory of Catalysis, Dalian Institute of Chemical Physics, Chinese Academy of Sciences, Dalian 116023, China

Received August 1, 2006. Revised Manuscript Received November 11, 2006

In this work, we present a facile route to fabricate three-dimensionally ordered macroporous SiO_2/graphitized carbon, TiO_2/graphitized carbon, and the resultant graphitic carbon. The graphitized carbons were formed by catalytic graphitization of polystyrene arrays, which were used as both template and carbon source for the generation of macroporous composite. The prepared samples were characterized via powder X-ray diffraction, Raman spectroscopy, SEM, TEM, HRTEM, thermogravimetic analysis, and N_2 adsorption. The graphitization degree and the content of graphitic carbon in the composite were dependent on the pyrolysis temperature and confinement effect of macroporous oxides skeleton. The composite of SiO_2/graphitized carbon exhibited long-range ordered structure at the pyrolysis temperature ranging from 600 to 1000 °C. The low pyrolysis temperature leads to the low degree of graphitization and low content of graphitic carbon in the composite. After the SiO_2 skeleton was removed, depending on the carbon content and the graphitization extent in the SiO_2/graphitized carbon composite, the resultant graphitic carbons display either collapsed or ordered macroporous structure. Based on the HRTEM, the interlayer distance of graphitized carbon at a pyrolysis temperature of 900 °C is estimated to be 0.348 nm. In comparison with SiO_2/graphitized carbon, the composite of TiO_2/graphitized carbon exhibits less ordering but slightly higher surface area. The photoactivity of TiO_2/graphitized carbon was examined and compared to commercial P25 and the composite of TiO_2/amorphous carbon in terms of degradation of Rhodamine B and eosin Y aqueous solution. It was found the TiO_2/graphitized carbon showed higher activity than TiO_2/amorphous carbon and P25 in the degradation of Rhodamine B and activity comparable to that of P25 in the degradation of eosin Y.

1. Introduction

Nanostructured materials have received much attention due to their unusual optical, photoelectrochemical, and electronic properties. Porous carbon materials have potential applications as adsorbents,[1] catalyst supports,[2,3] and photonic materials.[4−6] The general procedure for the preparation of ordered carbon materials includes filling the interstices of template with an appropriate carbon precursor, carbonization of the composite at high temperature, and the subsequent template removal.[7] Among all kinds of carbon precursors, sucrose is perhaps the most commonly used carbon precursor.[5,8,9] Despite the narrow pore size distribution and high surface area, the walls of these porous carbons are usually amorphous. It is well known that the electronic property of the carbon is closely related to its graphitic nature, which, in many cases, determines the performance of the resulting carbon materials. For many advanced applications such as electrochemistry[10] and photocatalysis,[11] porous carbon with graphitic character is highly desirable because of its well-developed crystalline structure, high electronic conductivity, and improved thermal stability.

The precursors containing graphitic building blocks are potentially suitable for the synthesis of graphitized carbon materials. These precursors include polyaromatic hydrocarbons,[12] aromatic molecules,[13] mesophase pitches,[14−17] and

* Corresponding author. Tel.: 86-411-82156658. Fax: 86-411-82156858. E-mail: zblei@lnnu.edu.cn.
† Liaoning Normal University.
‡ Chinese Academy of Sciences.

(1) Han, S. J.; Sohn, K. K.; Hyeon, T. *Chem. Mater.* **2000**, *12*, 3337−3341.
(2) Chai, G. S.; Yoon, S. B.; Yu, J. S.; Choi, J. H.; Sung, Y. E. *J. Phys. Chem. B* **2004**, *108*, 7074−7079. Yu, J. S.; Kang, S.; Yoon, S. B.; Chai, G. S. *J. Am. Chem. Soc.* **2002**, *124*, 9382−9383.
(3) Chai, G. S.; Yoon, S. B.; Kim, J. H.; Yu, J. S. *Chem. Commun.* **2004**, 2766−2767.
(4) Zakhidov, A. A.; Baughman, R. H.; Iqbal, Z.; Cui, C. X.; Khayrullin, I.; Dantas, S. O.; Marti, J.; Ralchenko, V. G. *Science* **1998**, *282*, 897−901.
(5) Lei, Z. B.; Zhang, Y. G.; Wang, H.; Ke, Y. X.; Li, J. M.; Li, F. Q.; Xing, J. Y. *J. Mater. Chem.* **2001**, *11*, 1975−1977.
(6) Lei, Z. B.; Zhang, H. C.; Ma, S. H.; Ke, Y. X.; Li, J. M.; Li, F. Q. *Chem. Commun.* **2002**, 676−677.
(7) Lu, A. H.; Schüth, F. *Adv. Mater.* **2006**, *18*, 1793−1805. Lee, J.; Kim, J. Hyeon, T. *Adv. Mater.* **2006**, *18*, 2073−2094. Lee, J.; Han, S.; Hyeon, T. *J. Mater. Chem.* **2004**, *14*, 478−486. Zhao, X. S.; Su, F. B.; Yan, Q. F.; Guo, W. P.; Bao, X. Y.; Lv, L.; Zhou, Z. C. *J. Mater. Chem.* **2006**, *16*, 637−648.
(8) Ryoo, R.; Joo, S. H.; Jun, S. *J. Phys. Chem. B* **1999**, *103*, 7743−7746.
(9) Jun, S.; Joo, S. H.; Ryoo, R.; Kruk, M.; Jaroniec, M.; Liu, Z.; Ohsuna, T.; Terasaki, O. *J. Am. Chem. Soc.* **2000**, *122*, 10712−10713.
(10) Su, F. B.; Zhao, X. S.; Wang, Y.; Zeng, J. H.; Zhou, Z. C.; Lee, J. Y. *J. Phys. Chem. B* **2005**, *109*, 20200−20206.
(11) Shanmugam, S.; Gabashvili, A.; Jacob, D. S.; Yu, J. C.; Gedanken, A. *Chem. Mater.* **2006**, *18*, 2275−2282.

10.1021/cm061806m CCC: $37.00
Published on Web 12/30/2006

polyacrylonitrile.[18,19] The resulting graphitic mesostructured carbons fabricated by using aromatic hydrocarbons (e.g., naphthalene, anthracene, pyrene)[13] as precursor exhibit higher electronic conductivity in comparison with that synthesized by sucrose. The $AlCl_3$-catalyzed route developed by Ryoo and his co-workers was relatively complicated, and the repeated heating process was needed.[12] Mesoporous graphitized carbon using mesophase pitches as the precursor and mesoporous silica as hard template were independently synthesized by several groups.[14−17] N-doped graphitic mesoporous carbons were synthesized using acetonitrile as precursor and a variety of mesoporous silica as template. By changing the synthesis condition of chemical vapor deposition (CVD),[20−22] both the morphology and the pore size of the resulting graphitic carbons can be simultaneously controlled. Highly graphitized carbons with pores size on the border between mesopores and macropores were achieved by the colloidal crystal template method, which required an extremely high graphitization temperature of 2400 °C.[17] Thus, the facile and effective synthetic strategies to the ordered porous graphitized carbon at low synthesis temperature remain an interesting topic and are still expected.

Three-dimensionally ordered macroporous (3DOM) materials are technologically important for many applications,[23,24] such as photonic crystals because of the optical length scale periodicity, or as catalysis supports due to their 3D interconnected windows, which allow for the efficient mass transport of the reactant and the product molecules. For example, the Pt−Ru catalyst supported on the macroporous carbon and the Pt catalyst supported on graphitized macroporous carbon showed improved activity for methanol oxidation than that supported on the generally used commercial E-TEK and Vulcan XC-72 supports.[2,3,10] Moreover, it was observed the macroporous carbon having graphitic nature could enhance the rate performance and cyclability in lithium-ion batteries.[10] The higher catalytic activity was ascribed to the higher surface area, graphitic nature, and the interconnected macroporous structure. 3DOM carbon doped with metal nanoparticles was fabricated via the base-catalyzed sol−gel method,[25] but the pore wall of graphitic character was not investigated. Zhao and his co-workers reported the fabrication of macroporous carbon, carbon capsules, and carbon spheres using inverse silica opal as the template,[10,26] which is a typical two-step process. Heterogeneous catalytic pyrolysis in the presence of transition metal was widely used to generate carbon materials with graphitic network at relatively low temperature.[27−29] For instance, catalytic graphitization of carbon aerogels by transition metals (Cr, Mn, Fe, Co, or Ni) produced graphitic nanoribbons with different curvatures,[30] graphitized domains with three-dimensional stacking order,[31] nanocoils displaying superior electrocatalytic activity for methanol oxidation,[32] and graphitized mesoporous carbons exhibiting high electrical conductivities.[33] Graphite-protected cobalt nanoparticles prepared by pyrolyzing surfactant-functionalized cobalt nanoparticles were found to be highly stable under strong acidic and basic conditions.[34] To our knowledge, catalytic graphitization with the aid of transition metals was not applied for the fabrication of 3DOM graphitized carbon. In the conventional fabrication of 3DOM materials, the PS arrays were often used as templates, which were usually removed by calcinations of the composite in air[35−37] or solvent extraction.[38,39] Recently, it was reported that styrene and polystyrene could be used as the carbon source to generate graphitized mesopores carbon.[21,40] In the present work, we report a facile method to fabricate 3DOM SiO_2/graphitized carbon, TiO_2/graphitized carbon (denoted as SiO_2/GC and TiO_2/GC in the following text, respectively) composite, and the resultant 3DOM graphitized carbon via in-situ pyrolysis of nickel-impregnated polystyrene arrays. The influence of pyrolysis temperature was investigated on the extent of graphitization as well as the ordering of the resultant graphitic carbons. The long-range ordering was observed for all composites of SiO_2/GC pyrolyzed at the temperature range of 600−1000 °C. The structure of the resultant graphitic carbon, which was obtained by removing the SiO_2 skeleton from the SiO_2/GC composite, depends on the graphite content and the graphitization degree in the corresponding SiO_2/GC composite. The photoactivity of

(12) Kim, T.-W.; Park, I.-S.; Ryoo, R. *Angew. Chem., Int. Ed.* **2003**, *42*, 4375−4379.
(13) Kim, C. H.; Lee, D.-K.; Pinnavaia, T. J. *Langmuir* **2004**, *20*, 5157−5159.
(14) Yang, H. F.; Yan, Y.; Liu, Y.; Zhang, F. Q.; Zhang, R. Y.; Meng, Y.; Li, M.; Xie, S. H.; Tu, B.; Zhao, D. Y. *J. Phys. Chem. B* **2004**, *108*, 17320−17328.
(15) Li, Z. J.; Jaroniec, M.; Lee, Y.-J.; Radovic, L. R. *Chem. Commun.* **2002**, 1346−1347.
(16) Li, Z. J.; Jaroniec, M. *J. Phys. Chem. B* **2004**, *108*, 824−826.
(17) Yoon, S. B.; Chai, G. S.; Kang, S. K.; Yu, J. S.; Gierszal, K. P.; Jaroniec, M. *J. Am. Chem. Soc.* **2005**, *127*, 4188−4189.
(18) Kruk, M.; Dufour, B.; Celer, E. B.; Kowalewski, T.; Jaroniec, M.; Matyjaszewski, K. *J. Phys. Chem. B* **2005**, *109*, 9216−9225.
(19) Lu, A. H.; Kiefer, A.; Schmidt, W.; Schüth, F. *Chem. Mater.* **2004**, *16*, 100−103.
(20) Xia, Y. D.; Yang, Z. X.; Mokaya, R. *Chem. Mater.* **2006**, *18*, 140−148.
(21) Xia, Y. D.; Mokaya, R. *Adv. Mater.* **2004**, *16*, 1553−1558.
(22) Xia, Y. D.; Mokaya, R. *Chem. Mater.* **2005**, *17*, 1553−1560.
(23) Stein, A. *Microporous Mesoporous Mater.* **2001**, *44*, 227−239.
(24) Velev, O. D.; Lenhoff, A. M. *Curr. Opin. Colloid Interface Sci.* **2000**, *5*, 56−63.
(25) Baumann, T. F.; J. H., Jr. *Chem. Mater.* **2003**, *15*, 3745−3747.
(26) Zhou, Z. C.; Yan, Q. F.; Su, F. B.; Zhao, X. S. *J. Mater. Chem.* **2006**, *15*, 2569−2574.
(27) Lu, A. H.; Li, W. C.; Salabas, E.-L.; Spliethoff, B.; Schüth, F. *Chem. Mater.* **2006**, *18*, 2086−2094.
(28) Kasahara, N.; Shiraishi, S.; Oya, A. *Carbon* **2003**, *41*, 1654−1656.
(29) Mochida, I.; Ohtsubo, R.; Takeshita, K.; Marsh, H. *Carbon* **1980**, *18*, 117−123.
(30) Fu, R. W.; Baumann, T. F.; Cronin, S.; Dresselhaus, G.; Dresselhaus, M. S.; J. H., Jr. S. *Langmuir* **2005**, *21*, 2647−2651.
(31) Maldonado-Hódar, F. J.; Moreno-Castilla, C.; Rivera-Utrilla, J.; Hanzawa, Y.; Yamada, Y. *Langmuir* **2000**, *16*, 4367−4373.
(32) Hyeon, T. Y.; Han, S. J.; Sung, Y.; Park, K.; Kim, Y. *Angew. Chem., Int. Ed.* **2003**, *42*, 4352−4356.
(33) Sevilla, M.; Fuertes, A. B. *Carbon* **2006**, *44*, 468−474.
(34) Lu, A. H.; Li, W. C.; Matoussevitch, N.; Spliethoff, B.; Bönnemann, H.; Schüth, F. *Chem. Commun.* **2005**, 98−100.
(35) Yan, H. W.; Blanford, C. F.; Holl, B. T.; Smyrl, W. H.; Stein, A. *Chem. Mater.* **2000**, *12*, 1134−1141.
(36) Lei, Z. B.; Li, J. M.; Zhang, Y. G.; Lu, S. M. *J. Mater. Chem.* **2000**, *10*, 2629−2631.
(37) Zhang, Y. G.; Lei, Z. B.; Li, J. M.; Lu, S. M. *New J. Chem.* **2001**, *25*, 1118−1120.
(38) Gu, Z. Z.; Hayami, S.; Kubo, S.; Meng, Q. B.; Einaga, Y.; Tryk, D. A.; Fujishima, A.; Sato, Q. *J. Am. Chem. Soc.* **2001**, *123*, 175−176.
(39) Tessier, P. M.; Velev, O. D.; Kalambur, A. T.; Rabolt, J. F.; Lenhoff, A. M.; Kaler, E. M. *J. Am. Chem. Soc.* **2000**, *122*, 9554−9555.
(40) Mbileni, C. N.; Prinsloo, F. F.; Witcomb, M. J.; Coville, N. J. *Carbon* **2006**, *44*, 1476−1483.

TiO_2/GC was examined and compared to that of commercial P25 and TiO_2/amorphous carbon composite in terms of degradation of Rhodamine B and eosin Y aqueous solution.

2. Experimental Section

2.1. Formation of SiO_2/GC and TiO_2/GC Composites. The preparation procedure in this work is described as follows. First, monodisperse polystyrene (PS) spheres with diameters of 580 and 620 nm were prepared by emulsifier-free emulsion polymerization using potassium persulfate as the anionic initiator.[41] Typically, 21 mL of freshly distilled styrene was added at 70 °C to 200 mL of deionized water, which was purged with argon before the reaction. Next, 0.3 g of potassium persulfate was added to the solution. The mixture was stirred at 70 °C for 30 h. The obtained PS colloidal spheres were rinsed with ethanol solution and allowed to self-assemble via vertical deposition technique. Next, 0.8 g of assembled PS arrays was impregnated with 4.8 mL of 0.086 mmol/mL $Ni(NO_3)_2$ ethanol solution (50% V/V) and dried at 45 °C. For the preparation of SiO_2/graphitized carbon, the interstices between PS arrays were infiltrated with the silica sol, which was prepared by mixing 0.6 mL of tetraethylorthosilicate (TEOS), 0.13 mL of water, 0.12 mL of 0.1 mol/L HCl solution, and 1.5 mL of absolute ethanol. In case of TiO_2/GC, the titanic precursor was prepared by diluting 0.7 mL of titanium tetrabutoxide in 1 mL of absolute ethanol. After hydrolysis and condensation at 45 °C overnight, the composite of oxides gel and PS arrays was subjected to preliminary pyrolysis in the flowing Ar at 300 °C for 2.5 h and then to the desired pyrolysis temperature (from 600 to 1000 °C) for further 3 h. The final composite was designated as SiO_2/GC-X or TiO_2/GC-X, where X is the pyrolysis temperature. The graphitic carbon was obtained by removing SiO_2 from SiO_2/GC composite with 20% hydrofluoric (HF) acid solution (*Caution: HF acid is highly corrosive, and the etching must be handled with care*). The resultant graphitic carbon was designated as GC-X, where X is the pyrolysis temperature of the composite.

2.2. Structure Characterization. The X-ray diffraction measurements were carried out on a Bruker AXS D Advance powder X-ray diffractometer with a Cu Kα ($\lambda = 1.5418$ Å) radiation source, operating at 40 kV and 40 mA. Diffraction patterns were collected from 10° to 80° at a speed of 3°/min. Scanning electron microscopy of the sample was carried out on a KYKY-1000B scanning electron microscope operating at 25 kV. The diameter of the pore size and the wall thickness of the composite were determined from SEM images. The sample morphology was observed on an FEI TECNAI G^2 F30 field-emission high-resolution transmission electron microscope, working at a 300 kV accelerating voltage. Acton Raman spectrometer was used to investigate the nature of the carbon in the composite, using the 532 nm laser line as the excitation source. Thermogravimetic analysis was performed on the Perkin-Elmer Diamond TG/DTA analyzer. The measurement was carried out under air atmosphere from room temperature to 900 °C, with a heating rate of 10 °C/min. The structure of the sample was characterized by nitrogen adsorption at 77 K using a Quantachrome Autosorb-1 analyzer. Before measurement, all samples were degassed at 200 °C for 6 h. The surface area was calculated using the BET method based on the adsorption data in the relative pressure (P/P_0) of 0.05−0.2.

2.3. Photocatalytic Activity Measurement. The photocatalytic activity of the TiO_2/GC was evaluated for the degradation of Rhodamine B and eosin Y aqueous solution under UV light irradiation. Before the reaction, the TiO_2/GC catalyst was rinsed with toluene and benzene to remove the byproducts adsorbed on the surface of catalyst during the pyrolysis process. A cylindrical flask (capacity ca. 250 mL) was used as the photoreactor vessel. About 50 mg of catalyst for degradation of rhodamine B or 35 mg of catalyst for degradation of eosin Y was magnetically stirred in a reactant solution, which contains 130 mL of Rhodamine B with initial concentration of 5.4×10^{-5} M or eosin Y with initial concentration of 5.0×10^{-4} M. Before irradiation, the solution was stirred in the dark for 20 min to reach the adsorption equilibrium of dye with the catalyst. The solution was irradiated by a 125 W high-pressure Hg lamp, which was placed in an inner irradiation cell made of quartz. TiO_2/amorphous carbon and commercially available TiO_2 (Degussa P25) were used as the reference with which to compare the photocatalytic activity under the identical experiment conditions. The degradation rate was determined at different intervals by UV−vis spectroscopy, using the characteristic maximum absorption of 554 and 515 nm as the monitored parameter for Rhodamine B and eosin Y, respectively.

Scheme 1. Synthetic Procedure of SiO_2/GC, TiO_2/GC, and the Resultant Graphitized Carbon with Ordered Macroporous Structure

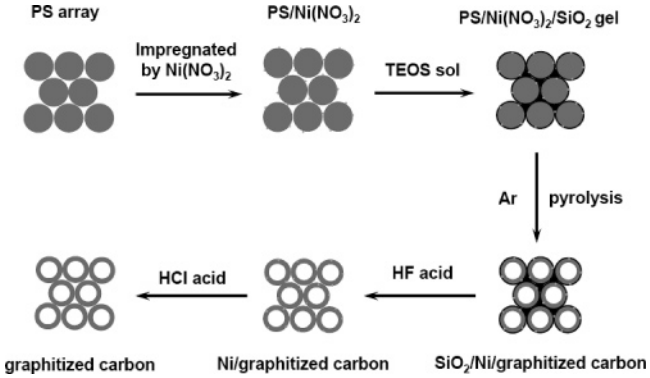

3. Results and Discussion

3.1. Formation of Graphitized Carbon during the Pyrolysis Process. The preparation procedure for 3DOM SiO_2/GC, TiO_2/GC, and the resultant graphitic carbon was schematically described in Scheme 1. $Ni(NO_3)_2$ impregnated ordered PS arrays were infiltrated with the precursor (SiO_2 or TiO_2) sol, followed by the hydrolysis and condensation to generate the composite of oxides gel and PS arrays. During the pyrolysis process, the following chemical reactions took place in the composite. The SiO_2 or TiO_2 gel transformed into the corresponding oxide in the interstices of PS arrays, and the ordered macroporous skeleton was established. $Ni(NO_3)_2$ decomposed into NiO, and then NiO was reduced into Ni particles at ~400 °C.[30] The PS arrays were carbonized and converted into amorphous carbon in flowing Ar gas. The amorphous carbon crystallized into graphitized carbon with the assistance of nickel and then deposited on the pore wall of SiO_2 or TiO_2 to constitute the final SiO_2/GC or TiO_2/GC composite. The graphitized carbon was obtained by removing SiO_2 from SiO_2/GC composite in HF solution. The present route is simple and facile for the fabrication of graphitized carbon with 3DOM structure. This method allows the graphitic carbon to be formed via in-situ conversion of carbonized PS arrays, different from the previously reported two-step process, in which the prelimi-

(41) Wang, P.; Chen, D.; Tang, F. Q. *Langmuir* **2006**, *22*, 4832−4835.

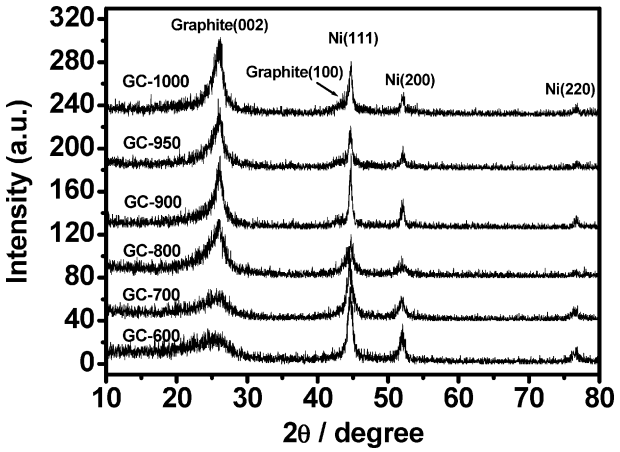

Figure 1. Powder X-ray diffraction patterns of the resultant graphitized carbon synthesized at different pyrolysis temperatures.

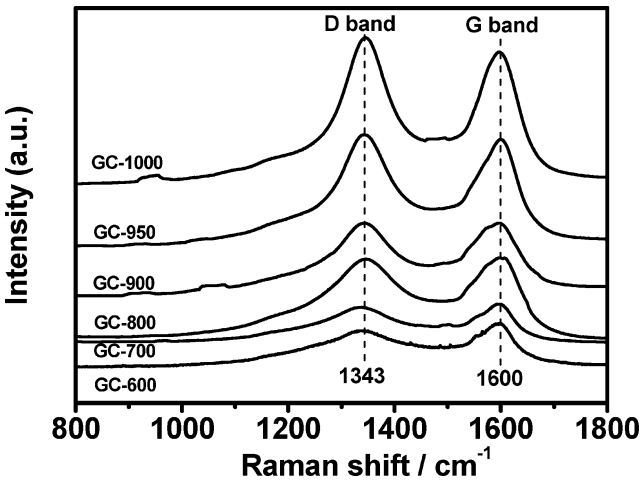

Figure 2. Raman spectra of the resultant graphitized carbon synthesized at different pyrolysis temperatures.

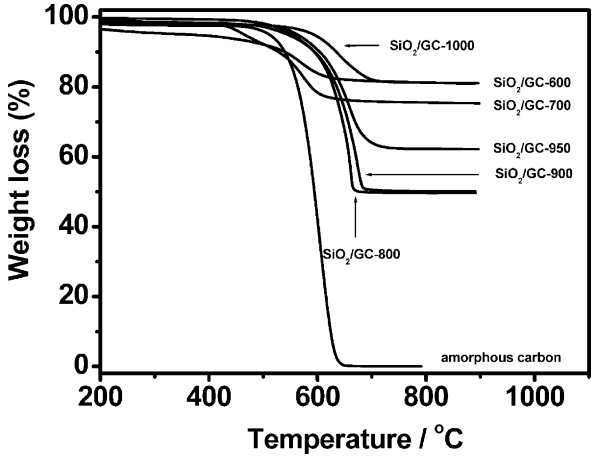

Figure 3. Thermogravimetric curves of the SiO_2/GC composite synthesized at different pyrolysis temperatures. For comparison, thermogravimetric curves of amorphous mesoporous carbon synthesized by using sucrose as carbon source[43] were also provided.

nary carbonization of precursor and the subsequent graphitization by transition metal were separated.[17,33]

Figure 1 shows the XRD patterns of graphitized carbon fabricated at different pyrolysis temperatures. The broad peak at $2\theta = 26°$ was observed for sample prepared at 600 °C, a lower pyrolysis temperature in comparison with graphitized carbon prepared from phenolic resin precursor via a two-step process.[33] This observation indicated that the conversion of amorphous carbon into graphitized carbon started at a relatively low temperature. The peaks at 44.8°, 52°, and 76.8° are characteristic of cubic Ni, confirming that Ni particles were formed due to the reduction effect of carbon.[30] The diffraction peaks at $2\theta = 26°$ and 43° could be clearly observed as the pyrolysis temperature increased to 800 °C. These peaks were indexed to the (002) and (100) diffractions of the graphitic framework, respectively. Further increasing the pyrolysis temperature up to 1000 °C did not cause any significant variation in the intensity of (002) diffraction peak, suggesting that the degree of graphitization remained roughly comparable for all samples synthesized at the pyrolysis temperature in the range of 900−1000 °C. Similar results was also observed in the synthesis of mesoporous carbon using styrene as the carbon source,[21] presumably related to the inherent nature of styrene molecules. On the other hand, if the pyrolysis process was performed in the absent of Ni particles, a very weak peak at 26° was observed only when the pyrolysis temperature exceeded 900 °C. No diffraction peaks ascribed to the graphite nature were detected at a pyrolysis temperature below this temperature. Therefore, the presence of Ni is crucial for the conversion of amorphous carbons into graphitized carbons at low temperature. For the GC-900 sample, based on the Bragg formula and Scherrer equation, the interlayer distance value (d_{002}) between graphene planes was 0.343 nm, and the thickness of graphite domains was estimated to be 5.9 nm. In comparison with single crystals of graphite (0.335 nm),[42] the larger interlayer distance of our sample may arise from its low pyrolysis temperature.

The nature of graphitized carbon in the SiO_2/GC composite was also confirmed by Raman spectra. Figure 2 shows the Raman spectra of carbon sample prepared at different temperatures. All samples exhibit two peaks around 1343 and 1600 cm^{-1}, which are characteristic of a symmetry breakdown at the edge of graphene sheets (D band) and the E_{2g} vibrational mode of graphite layers (G band),[42] respectively. The presence of the G band provides evidence for the graphitic character of our sample. In comparison with the single crystals of graphite (1575 cm^{-1}), the G band of all samples shifted to higher wave numbers, indicating a structural imperfection of the graphene sheets of our sample.[10,42] The degree of graphitization can be estimated by comparing the relative intensity of the D band and G band. Despite the high pyrolysis temperature of 1000 °C, the observed two peaks showed comparable intensity, which is in accordance with the XRD result shown in Figure 1. This observation suggests there is still a noticeable amount of disordered graphite-like carbon in the sample even at a pyrolysis temperature of 1000 °C.

It is generally considered that the graphitized carbons with a higher graphitization should show more stable property against air oxidation. To evaluate the thermal stability and the graphite content in the SiO_2/GC composite, thermogravimetric (TG) weight losses were recorded in air from room temperature to 900 °C. Figure 3 displays the TG curves of SiO_2/GC composite synthesized at different pyrolysis tem-

(42) Tuinstra, F.; Koenig, J. L. *J. Chem. Phys.* **1970**, *53*, 1126−1130.

Table 1. Physical Properties of SiO_2/GC Synthesized at Different Temperatures

sample	macropore diameter (nm)[a]	wall thickness (nm)[a]	BET surface area (m^2/g)[b]	carbon content (%)[c]	temperature range of weight loss[c] (°C)
SiO_2/GC-600	389	135	38.7	13.2	420−640
SiO_2/GC-700	346	156	25.3	22.3	415−650
SiO_2/GC-800	338	159	23.4	48.2	480−680
SiO_2/GC-900	332	158	22.5	48.9	500−730
SiO_2/GC-950	312	167	24.2	35.4	510−740
SiO_2/GC-1000[d]	351	186	23.2	16.6	520−740

[a] Average macroporous diameter and wall thickness were determined from the SEM images. [b] Calculated on the basis of the adsorption data in the relative pressure (P/P_0) of 0.05−0.2. [c] Carbon content was determined on the basis of the mass of the initial PS arrays and the TG analysis; the temperature ranges of weight loss were obtained from TG analysis. [d] Using PS spheres with diameter of ∼620 nm as the template.

peratures. The sucrose-derived mesoporous carbon[43] with amorphous wall was also provided for comparison. The oxidation temperature of SiO_2/GC was found to shift toward the higher temperature range. This shift indicates the samples synthesized at higher pyrolysis temperature generally possess a higher degree of graphitization, in accordance with the XRD and Raman results. Table 1 lists the oxidation temperature range of different SiO_2/GC samples. It was found the oxidation temperature of SiO_2/GC composite increased with the increase of pyrolysis temperature and then retained in a roughly invariable range (500−740 °C). For example, the SiO_2/GC-600 with low graphitization exhibits an oxidation temperature range similar to that of amorphous mesoporous carbon. This lower oxidation temperature is associated with the imperfect structure of the graphene layers.[44] In contrast, the oxidation temperature range of SiO_2/GC-900 is increased to 500−730 °C, suggesting its higher graphitization property. Calculated from the TG curve as well as the initial weight of PS arrays, the production yield of graphitized carbon varies from ∼7% for SiO_2/GC-600 to ∼15% for SiO_2/GC-900, which is rather lower than that of graphitic carbons using mesophase pitches as carbon precursor.[14] In addition, the graphite content in the SiO_2/GC composite is also dependent on the pyrolysis temperature. This phenomenon appears as the result of confinement effects of macroporous oxides skeleton, which will be discussed later.

3.2. Pore Structure of SiO_2/GC. The pore structure of the resulting SiO_2/GC was observed on a scanning electron microscope. Figure 4A−F shows SEM images of the SiO_2/GC composite with pyrolysis temperature increased from 600 to 1000 °C. The three-dimensionally periodic structure with long-range ordering was observed for all of the composite samples. This ordered framework was derived from the long-range ordering of the initial PS arrays, suggesting that the PS arrays were essentially functionalized as the template for the generation of ordered macroporous composite. The size of spherical pores is dependent on the diameter of initial PS spheres, as well as the pyrolysis temperature. As listed in Table 1, the macroporous composite with pore size varying from 312 to 389 nm could be obtained using 580 nm PS

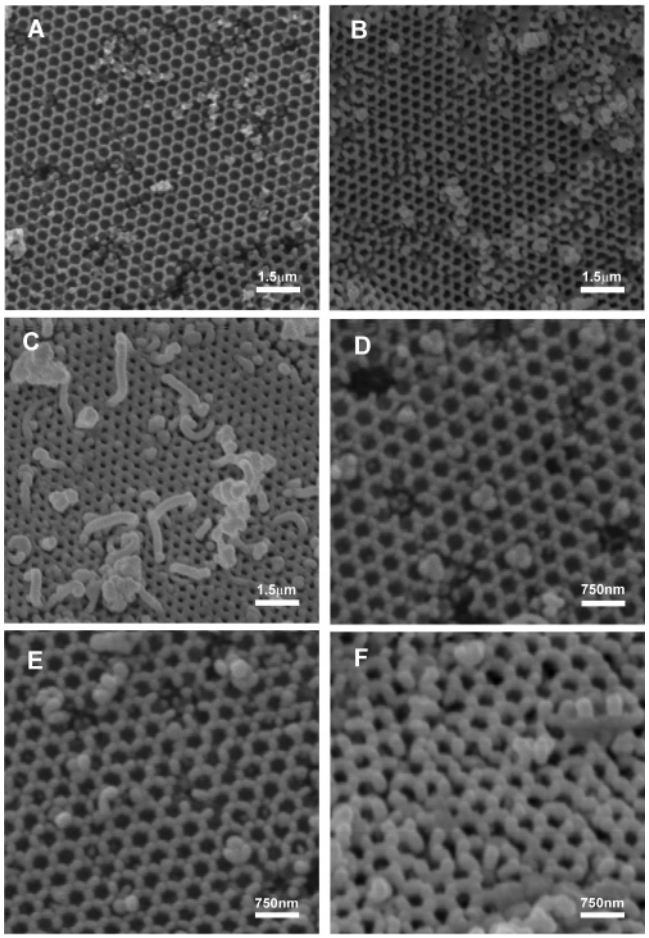

Figure 4. SEM images of 3DOM SiO_2/GC composite synthesized at different pyrolysis temperatures: (A) 600, (B) 700, (C) 800, (D) 900, (E) 950, and (F) 1000 °C.

spheres as template. The higher pyrolysis temperature leads to the macropores with decreased pore size, which was due to structure shrinkage during the pyrolysis process. On the other hand, the higher pyrolysis temperature leads to the SiO_2/GC composite with increased wall thickness, which mainly arose from the high-temperature sintering. As can be seen in these images, the composite synthesized at lower pyrolysis temperature exhibits a smooth pore wall with fewer defects and fractures (Figure 4A). However, seriously lattice distortions and coarse pore wall due to the high-temperature sintering were observed for sample fabricated at pyrolysis temperature above 950 °C (Figure 4E, F). At this temperature, the macroporous SiO_2 skeleton begins to interpenetrate through viscous flow[45] and leaves partial carbonized PS spheres uncovered with SiO_2 skeleton, which is detrimental to the deposition of graphitized carbon on the pore wall. This observation was supported by the sharply reduced graphite content in the composite as listed in Table 1. The graphite content in the composite, calculated from TG analysis, underwent the maximum value of 48.9 wt % at the pyrolysis temperature of 900 °C and then declined to 35.4 and 16.6 wt % at 950 and 1000 °C, respectively. This variation was attributed to the confinement effect of macroprous SiO_2 skeleton. We intentionally pyrolyzed the $Ni(NO_3)_2$-impregnated PS

(43) Lei, Z. B.; Xiao, Y.; Dang, L. Q.; Lu, M.; You, W. S. *Microporous Mesoporous Mater.* **2006**, *96*, 127−134.
(44) Bakandritsos, A.; Simopoulos, A.; Petridis, D. *Chem. Mater.* **2005**, *17*, 3468−3474.
(45) Míguez, H.; Meseguer, F.; Lopez, C.; Blanco, A.; Moya, J. S.; Requena, J.; Mifsud, A.; Fornes, V. *Adv. Mater.* **1998**, *10*, 480−483.

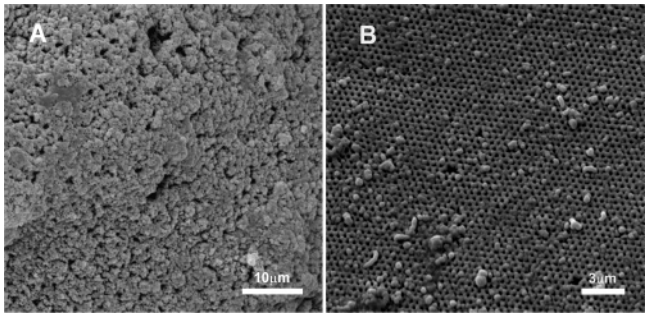

Figure 5. SEM images of the resultant graphitized carbon synthesized at pyrolysis temperatures of 600 (A) and 800 °C (B).

arrays without TEOS infiltration. Only a trace amount of product was obtained, and most of the gaseous carbon precursor species that arose from the polystyrene sphere were deposited on the surface of the quartz tube. This confinement effect was also observed in the preparation of partially graphitized carbon by carbonizing the silica/surfactant composite.[46] This finding shows the PS arrays surrounded by the integrated macroporous SiO_2 skeleton can effectively restrain the thermal decomposition of carbonized PS arrays and facilitate the subsequent conversion of amorphous carbon into graphitic carbon with the assistance of Ni particles.

The graphitization degree and the graphite content in the composite influence the structure of the resultant graphitic carbon. Figure 5 shows the SEM images of graphitized carbon with SiO_2 removed by HF acid solution. It is seen that the GC-600 sample exhibits a structure quite different from that of GC-800. The GC-800 sample retained the well-ordered structure of the parent SiO_2/GC-800. However, the 3DOM structure was lost for GC-600 after the SiO_2 skeleton was removed. This collapsed structure was also observed for the GC-700 sample (not shown). The different structure between GC-800 and GC-600 is relevant to the different graphitization extent and the graphite content in their corresponding parent SiO_2/GC composite. It is noted that the porous carbons with graphitic wall should show improved mechanical strength in comparison with amorphous carbons. SiO_2/GC composite synthesized at low pyrolysis temperature exhibited low graphitization and low graphite content, as indicated by XRD and TG analysis. For SiO_2/GC-600 and SiO_2/GC-700, the insufficient graphitization leads to graphitic wall with low mechanical strength. The low graphite content in the composite suggests a thin layer of graphitized carbon deposited on the SiO_2 pore walls. Both of the two factors lead to the collapsed structure of GC-600 and GC-700. In contrast, relatively high graphitization and higher graphite content in SiO_2/GC-800 composite provide enough strength to support its ordered structure after SiO_2 skeleton removal. The long-range ordered structure of graphitic carbon could be maintained at a pyrolysis temperature as high as 950 °C. The pore structure of GC-1000, however, was less ordered than that of GC-950 (Figure 1S in the Supporting Information). This less ordered structure was due to its low graphite content, although GC-1000 has a graphitization degree comparable to that of GC-950.

(46) Zhang, Y.; Hu, G.; O'Hare, D.; Wu, D.; Sun, Y. H. *Carbon* **2006**, *44*, 1969−1973.

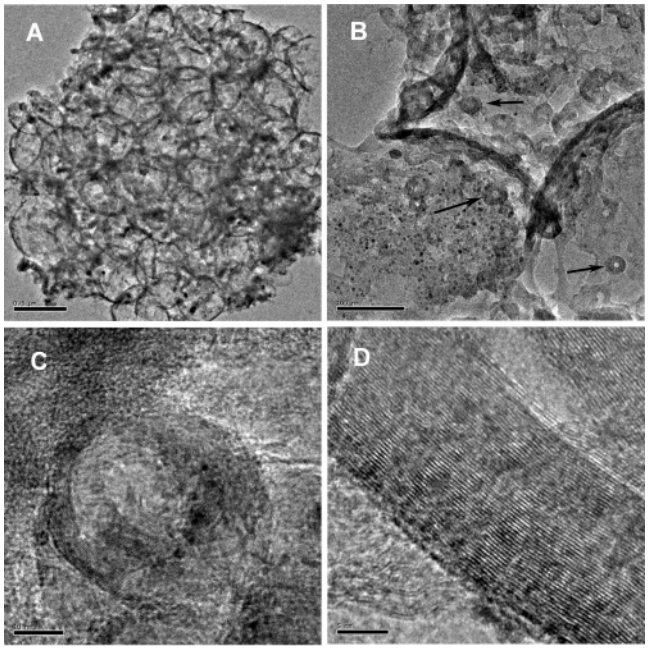

Figure 6. TEM images (A, B) and HRTEM images (C, D) of the resultant GC-900.

Figure 6 shows the TEM (A and B) and HRTEM (C and D) images of GC-900. It is evident that the pores are interconnected and close-packed, roughly spherical with a diameter of ∼490 nm. The wall thickness is estimated to be 15−40 nm. Nickel particles with size of 5−30 nm were homogeneously dispersed in the matrix of graphitic carbon, as shown in images A and B. Based on the TG analysis, the mass fraction of metal Ni in the graphitic carbon was estimated to be ∼12 wt %, supposing all metal Ni was oxidized into NiO. Besides the spherical macropores, there are a large number of coils randomly distributed in the matrix of macroporous graphitic carbon, as indicated by the arrows in Figure 6B. The thickness of the coils varies from 12 to 15 nm. It should be noted that these nanocoils were observed for all graphitized carbon synthesized at pyrolysis temperature in the range of 600−1000 °C, which confirmed the conversion of amorphous carbon into graphitized carbon started at the relatively low pyrolysis temperature of 600 °C. Similar nanocoils nanostructure was previously observed in the catalytic graphitization of the resorcinol−formaldehyde gel by the mixture of cobalt and nickel.[32] The HRTEM image of one single nanocoil shown in Figure 6C displays well-aligned graphitic layers, which corroborated the graphitic character. The HRTEM image (Figure 6D) taken from the edge of macropore wall reveals that the graphene layers are tightly stacked. The interlayer distance calculated from the histogram diagram shown in Figure 2S was estimated to be 0.348 nm, in agreement with the value calculated from the Bragg formula.

The wall structure of macroporous SiO_2/GC and the resultant macroporous graphitized carbon were also characterized by nitrogen adsorption. All samples display a type-II isotherm, characteristic of macroporous materials.[35] As summarized in Table 1, the BET surface area of SiO_2/GC varied from 22 to 38 m^2/g. Figure 3S shows the representative adsorption isotherm of GC-900 and SiO_2/GC-900. For both of them, the gradually increased adsorption with the

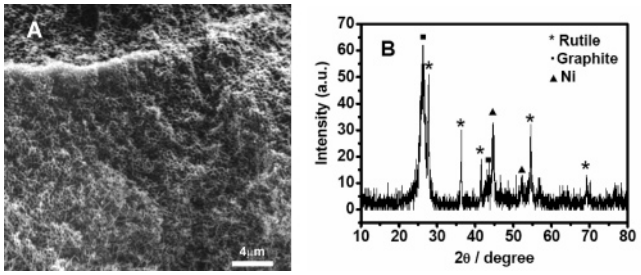

Figure 7. SEM image (A) and the powder X-ray diffraction patterns (B) of the TiO_2/GC-850 composite.

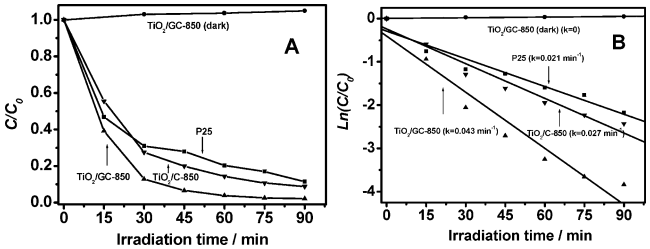

Figure 8. Photocatalytic degradation of Rhodamine B in the presence of macroporous TiO_2/GC-850, TiO_2/C-850, or commercial P25 (A) and the respective apparent first-order rate constant determined from the linear graph of $\ln(C/C_0)$ versus irradiation time (B). Light source, 125 W Hg lamp; Rhodamine B concentration, 5.4×10^{-5} M; catalyst, 50 mg.

increase of relative pressure is associated with the unrestricted monolayer−multilayer adsorption on the surfaces of macroporous or nonporous materials. For SiO_2/GC fabricated at 600−1000 °C, it is observed that the adsorption and desorption branches almost coincide at high relative pressure, indicating the nearly nonporous character of the pore wall. On the other hand, the evident hysteresis loop observed in the relative pressure ranging from 0.4 to 0.9 for GC-900 corresponds to the capillary condensation in the mesopores, suggesting the existence of textural mesopores on the macroporous wall of graphitized carbon. The distinct difference in adsorption amount between SiO_2/GC-900 and GC-900 brings about the large difference in surface area. The BET surface area of SiO_2/GC-900 is 22.5 m^2/g, which increased to 167 m^2/g for GC-900. The increased surface area arose from the mesoporous and macroporous cavities, which were created by the dissolving of SiO_2 skeleton from SiO_2/GC-900. This finding suggests, besides filling the interstices of PS arrays, the silica sol also penetrates into the matrix of PS spheres in the infiltration process.

3.3. Pore Structure of TiO_2/GC and Photoactivity. TiO_2 is one of the most important semiconductors used as photonic crystals, solar cells, and photocatalysts for the degradation of organic compounds. The combination of TiO_2 with carbon materials was recently prepared with the aim to improve the photocatalytic performance of TiO_2. For example, TiO_2 nanoparticles coated on 3DOM carbon,[47] TiO_2/carbon composite,[48] or TiO_2@carbon core−shell nanoparticles[11] have been prepared and structurally characterized. Particularly, carbon nanotubes supported TiO_2 particles showed enhanced photoactivity in degradation of azo dye,[49] as the consequence of the strong interaction between carbon nanotubes and TiO_2 as well as the good electronic conductivity of carbon nanotubes. We followed the preparation procedure of SiO_2/GC to synthesize TiO_2/GC composite. The similar pyrolysis process allows the graphitized carbon to be formed and closely combined with TiO_2, which is one of the important factors contributing to its high photoactivity in the degradation of Rhodamine B and eosin Y aqueous solution.

Figure 7A shows the SEM image of the macroporous TiO_2/GC-850. Although the macroporous structure is still preserved during the pyrolysis process, the long-range ordering is poor in comparison with SiO_2/GC. This less ordering might arise from the phase transformation of TiO_2 from anatase to rutile. Figure 7B shows XRD patterns of TiO_2/GC-850, suggesting the coexistence of graphitized carbon, rutile, and the cubic nickel particles. Based on the TEM, the particle size of rutile in TiO_2/GC-850 is ∼30 nm. The amorphous carbon in TiO_2/carbonized PS composite also started to crystallize at 600 °C, a similar pyrolysis temperature in comparison with that of SiO_2/GC. The content of graphitic carbon in the TiO_2/GC-850 composite calculated from the TG analysis is ∼60 wt %, which is higher than that of SiO_2/GC. This difference is associated with the different interaction between carbonized PS and precursor, and the degree of pore confinement effect. The BET surface area of TiO_2/GC-850 is 49.5 m^2/g, also larger than the counterpart of SiO_2/GC.

The photoactivity of TiO_2/GC-850 was evaluated in the degradation of Rhodamine B aqueous solution. Moreover, the activity of TiO_2/GC-850 was compared to commercial P25 and the TiO_2/C-850 composite, which was prepared by pyrolyzing TiO_2/PS arrays without the assistance of Ni. Powder XRD confirmed the TiO_2/C-850 composite consists of amorphous carbon and rutile TiO_2. As shown in Figure 8A, the TiO_2/GC-850 exhibits more efficient activity in degradation of Rhodamine B than both TiO_2/C-850 and commercial P25, although the amount of TiO_2 in TiO_2/GC-850 is only 40 wt %. About 96% Rhodamine B was degraded within 60 min of irradiation in the presence of TiO_2/GC-850. In comparison, ∼86% and 80% Rhodamine B was degraded in the presence of TiO_2/C-850 and P25, respectively, within the same irradiation time. No evident degradation was observed in the dark for TiO_2/GC-850 catalyst, suggesting that the degradation of Rhodamine B proceeded via photocatalysis instead of the adsorption effect. The nickel particles in the TiO_2/GC-850 composite were found to have no noticeable contribution to the photoactivity. As can be seen in Figure 8B, the degradation of Rhodamine B followed apparent first-order reaction, and the rate constant was determined to be 0.043, 0.027, and 0.021 min^{-1} for TiO_2/GC-850, TiO_2/C-850, and P25, respectively.

Degussa P25 is one of the most commonly used reference photocatalysts, with which to compare the activity of other types of photocatalyst for the decomposition of dye or chlorophenol.[11,50−52] It is considered that the crystallinity and

(47) Wang, Z. Y.; Ergang, N. S.; Al-Daous, M. A.; Stein, A. *Chem. Mater.* **2005**, *17*, 6805−6813.
(48) Lee, S. W.; Sigmund, W. M. *Chem. Commun.* **2003**, 780−781.
(49) Yu, Y.; Yu, J. C.; Chan, C. Y.; Che, Y. K.; Zhao, J. C.; Ding, Y.; Ge, W. K.; Wong, P. K. *Appl. Catal., B: Environ.* **2005**, *61*, 1−11.
(50) Zhang, D. Y.; Yang, D.; Zhang, H. J.; Lu, C. H.; Qi, L. M. *Chem. Mater.* **2006**, *18*, 3477−3485.
(51) Shchukin, D. G.; Caruso, R. A. *Chem. Mater.* **2004**, *16*, 2287−2292.

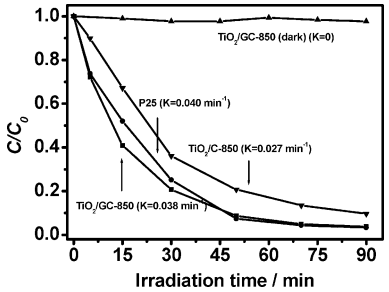

Figure 9. Photocatalytic degradation of eosin Y in the presence of macroporous TiO_2/GC-850, TiO_2/C-850, or commercial P25. Light source, 125 W Hg lamp; eosin Y concentration, 5.0×10^{-4} M; catalyst, 35 mg.

the surface area are dominative factors determining the performance of the catalyst. Commercial P25 consists of ~80% anatase and 20% rutile, with typical particle size of ~25 nm and BET surface area of 56 m^2/g, which was confirmed by powder XRD, TEM, and N_2 adsorption at 77 K. The surface area of TiO_2/GC-850 is 49.5 m^2/g, and rutile size in the composite was estimated to be ~30 nm based on the TEM. As compared to TiO_2/GC-850, the strong rutile peaks in the XRD pattern of TiO_2/C-850 (not shown) indicate the good crystallinity and larger particle size of rutile, ~53 nm based on the Scherrer equation. This increased rutile size leads to a slightly decreased surface area of 36.5 m^2/g. Although both the surface area and the crystallinity of TiO_2/C-850 and TiO_2/GC-850 were taken into account, TiO_2/GC-850 showed 1.6 times higher activity than TiO_2/C-850 according to the rate constant shown in Figure 8B. Thus, the moderate graphitization of the macroporous TiO_2/GC-850 may contribute to its higher photoactivity. It is known that the graphitized carbons exhibit improved electronic conductivity in comparison with amorphous carbon.[13,31] The good electronic conductivity of graphitized carbon, as well as the intimate contact between TiO_2 and graphitized carbon, facilitate rapid migration of the photoexcited electrons from the conduction band of TiO_2 to the graphitized carbon support, which reduces the recombination between electrons and holes and leaves more holes to participate in the oxidization reaction of dye molecules. In this respect, the photocatalysis mechanism is similar to the degradation of dye in the presence of carbon nanotubes-supported TiO_2.[49]

The photoactivity of TiO_2/GC-850 was also examined for degradation of eosin Y as shown in Figure 9. It is seen that the TiO_2/GC-850 composite also shows higher activity than TiO_2/C-850 and activity comparable to that of P25 under identical irradiation conditions. The degradation process is roughly the first-order reaction, which is consistent with the results obtained from the degradation of eosin B aqueous solution in the presence of nanoporous ZnS.[53] Based on the first-order rate constant, the photoactivity of the catalyst increases in the order of TiO_2/C-850 < TiO_2/GC-850 ≈ P25. It is evident that P25 shows a 2-fold higher activity in degradation of eosin Y than degradation of Rhodamine B under identical irradiation conditions. The detailed reason is not clear at present, possibly related to the different adsorption ability of dye molecules on the surface of P25 catalyst. Nevertheless, the rate constant of TiO_2/C-850 and TiO_2/GC-850 remains nearly invariable in the degradation of Rhodamine B and eosin Y. As compared to TiO_2/C-850, the higher activity of TiO_2/GC-850 is also the integrated results of surface area, crystallinity, as well as the graphitic nature with 3D interconnected pore structure.

4. Conclusions

The composites of SiO_2/graphitized carbon, TiO_2/graphitized carbon, and the resultant graphitized carbons with 3D ordered macroporous structure were fabricated by pyrolyzing the corresponding precursor and PS arrays with the assistance of nickel. The nickel particles play an important role in the catalytic graphitization of PS arrays. The graphitization degree of carbon, the ordered 3D structure, and the content of graphitized carbon in the composite were highly dependent on the pyrolysis temperature and the confinement effects of oxides skeleton. The higher pyrolysis temperature (above 950 °C) leads to the SiO_2/GC composite with low graphite content and coarse pore wall. Both the graphite content and the graphitization degree in the parent SiO_2/GC determine the structure of the resultant graphitized carbon. The SiO_2/GC with higher graphite content and high graphitization degree can generate graphite with macroporous structure. The TiO_2/GC fabricated by a similar procedure exhibits less ordering and slightly higher surface area in comparison with SiO_2/GC. The photoactivity of TiO_2/GC was examined and compared to that TiO_2/amorphous carbon and commercial P25. The higher activity of TiO_2/GC-850 in degradation of Rhodamine B and eosin Y aqueous solution is the integrated result of slightly high surface area, small particle size, and graphitic nature with 3D interconnected pore structure. The method presented in this work is suitable for the fabrication of other 3DOM composite of oxides/graphitized carbon by choosing the appropriate precursors and controlling the synthesis condition. The 3DOM SiO_2/GC, TiO_2/GC-850, and resultant graphitized carbon could open new possibilities for the technological applications in catalysis, fuel cell, photonic crystals, and porous electrode materials.

Acknowledgment. We thank Professor Can Li, in State Key Laboratory of Catalysis, Dalian Institute of Chemical Physics, Chinese Academy of Sciences, for helpful discussions and Dr. Xuming Wei for HRTEM measurements. We also acknowledge the Natural Science Foundation of Liaoning Province (Grant No. 2050798) and the Natural Science Foundation of Dalian city (Grant No. 2006J23JH019) for financial support of this work.

Supporting Information Available: SEM images, HRTEM-derived histogram, and nitrogen adsorption isotherms (PDF). This material is available free of charge via the Internet at http://pubs.acs.org.

CM061806M

(52) Shchukin, D. G.; Schattka, J. H.; Antonietti, M.; Caruso, R. A. *J. Phys. Chem. B* **2003**, *107*, 952−957.
(53) Hu, J. S.; Ren, L. L.; Guo, Y. G.; Liang, H. P.; Cao, A. M.; Wan, L. J.; Bai, C. L. *Angew. Chem., Int. Ed.* **2005**, *44*, 1269−1273.